JOURNAL OF MATERIALS SCIENCE 22 (1987) 1701–1706

Development and partial relaxation of internal stresses in thin TiC layers chemically vapour deposited on Fe–C substrates

W. G. SLOOF, R. DELHEZ, Th. H. DE KEIJSER, E. J. MITTEMEIJER
Laboratory of Metallurgy, Delft University of Technology, Rotterdamseweg 137, 2628 AL Delft, The Netherlands

TiC layers were chemically vapour deposited at 1273 K on Fe–C substrates with carbon contents between 0.06 and 1.20 wt % C. X-ray diffraction stress analyses showed that large compressive stresses are present in the TiC coatings and that small tensile stresses are present in the substrates. The stresses developed during cooling from the deposition temperature to room temperature, owing to the difference in thermal shrink between coating and substrate. However, stress relaxation was also evident. This was provoked by the phase transformation processes occuring in the substrate on cooling. Stress relaxation was hindered when grain-boundary cementite formed in the substrates. The stresses present in the TiC coatings on substrates without grain-boundary cementite can be predicted quantitatively.

1. Introduction

TiC coatings are widely used for their excellent wear and corrosion resistance. For example, coating of cutting and forming tools with TiC prolongs their lifetime considerably [1].

Chemically vapour deposited (CVD) TiC layers on steels exhibit large internal stresses [2–4]. These stresses control to a great extent the adherence of the layer to the substrate and can also influence the fracture, fatigue, wear and corrosion resistance of the coating-substrate composite [5]. However, a full understanding of the development of (residual) stresses in both coating and substrate is lacking.

This contribution concerns the stresses in the CVD TiC layers and in the corresponding Fe–C substrates as determined by X-ray diffraction without layer removal. The development and subsequent partial relaxation of the stresses are explained quantitatively.

2. Specimen preparation

Fe–C substrates, with carbon contents between 0.06 and 1.20 wt % C, were prepared from powders of iron (Ventron, 99.999 wt %) and graphite (Ventron, F.R.G., 99.5 wt %). All substrates (diameter 30 mm and thickness 10 mm) were mechanically polished (final stage 1 μm diamond), ultrasonically cleaned in ethanol, degreased with freon and etched in a 2% nital solution prior to coating with TiC.

The CVD process was carried out in a standard industrial reactor system (Bernex Co., Switzerland). TiC was deposited during 5 h at 1273 $\pm$ 5 K from H_2 gas with 3 vol % $TiCl_4$, at a total pressure of 6.7 kPa. However, a number of substrates were coated in a gas atmosphere containing also 3 vol % CH_4. In those cases not only carbon from the substrate, but also carbon from the gas atmosphere contributed to the TiC formation.

After layer deposition the specimens were allowed to cool in the reactor in a protective H_2 atmosphere; this took about 2 h.

3. X-ray diffraction strain and stress determination

X-ray diffraction stress determination according to the $\sin^2\psi$ method [6] is based on the following relation:

$$\varepsilon_{\phi,\psi}^{hkl} = \frac{d_{\phi,\psi} - d_0}{d_0} = S_1^{hkl}(\sigma_1 + \sigma_2) + \tfrac{1}{2}S_2^{hkl}\sigma_\phi \sin^2\psi \quad (1)$$

where $h\,k\,l$ are the indices of the Bragg reflection, $\varepsilon_{\phi,\psi}^{hkl}$ is the strain of the $(h\,k\,l)$ spacing in the direction (ϕ, ψ) (cf. Fig. 1), d is the spacing of the $(h\,k\,l)$ planes as obtained from the peak position of the Bragg reflection measured for the direction (ϕ, ψ), d_0 is the strain-free $(h\,k\,l)$ spacing, σ_1 and σ_2 are the principal stresses in the plane of the specimen surface ($\sigma_3 = 0$), $\sigma_\phi = \sigma_1\cos^2\phi + \sigma_2\sin^2\phi$ and S_1^{hkl} and $\frac{1}{2}S_2^{hkl}$ are the so-called X-ray elastic constants for the $(h\,k\,l)$ planes.

For the TiC coatings and the substrates investigated, a plot of $d_{\phi,\psi}$ against $\sin^2\psi$ (Fig. 2) indeed yields a straight line as prescribed by Equation 1. Without any knowledge about d_0, still an accurate stress σ_ϕ (error < 1%) can be obtained from the slope of the straight line, because, for that purpose, it is allowed to replace d_0 by $d_{\phi,\psi=0}$ in the denominator of Equation 1. For the specimens investigated it was experimentally verified that σ_ϕ did not depend on ϕ, which implies that

$$\sigma_1 = \sigma_2 = \sigma_\phi \equiv \sigma_\parallel \quad (2)$$

The X-ray elastic constants used for the TiC coatings were calculated from the single-crystal elastic

0022–2461/87 $03.00 + .12

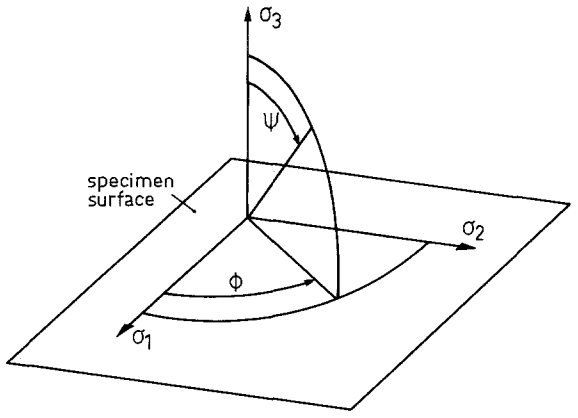

Figure 1 Definitions of angles ϕ and ψ. In the ω diffractometer ψ is measured along the ω circle.

constants of $TiC_{0.91}$ [7] by using the Eshelby–Kröner model [8]:

$$S_1^{hkl} = (-0.390 - 0.177\,\Gamma)10^{-6}\,\mathrm{MPa}^{-1} \quad (3)$$

$$\tfrac{1}{2}S_2^{hkl} = (2.55 + 0.53\,\Gamma)10^{-6}\,\mathrm{MPa}^{-1} \quad (4)$$

where $\Gamma = (h^2k^2 + k^2l^2 + l^2h^2)/(h^2 + k^2 + l^2)^2$. From Equations 3 and 4 it follows that TiC is elastically nearly isotropic.

The X-ray elastic constants used for the ferrite matrix of Fe–C substrates were calculated from the single-crystal elastic constants of pure iron [8] by using also the Eshelby–Kröner model:

$$S_1^{hkl} = (-1.88 + 2.54\,\Gamma)10^{-6}\,\mathrm{MPa}^{-1} \quad (5)$$

$$\tfrac{1}{2}S_2^{hkl} = (7.61 - 7.61\,\Gamma)10^{-6}\,\mathrm{MPa}^{-1} \quad (6)$$

Numerical values for the elastic constants used in the present investigation are given in Table I.

For the stress measurements Siemens ω diffractometers (type F and D500), with a graphite monochromator in the diffracted beam, were employed. The equipment settings for the reflections chosen are given in Table II. During the stress measurements, the specimens were rotated around an axis perpendicular to the specimen surface (cf. Equation 2). The choice of the reflections was mainly based on constraints of (i) minimal overlap with adjacent reflections, and (ii) large 2θ values to obtain a high accuracy in the determination of the lattice spacings and to be able to reach a large specimen tilt (ψ in Fig. 1) in the ω diffractometers.

TABLE I The elastic constants, at room temperature, and the linear expansion coefficient, α, used for the TiC coatings and the Fe–C substrates. The X-ray elastic constants, S_1^{hkl} and $\frac{1}{2}S_2^{hkl}$, Young's modulus, E, and Poisson ratio, ν, were obtained from the single-crystal elastic constants of $TiC_{0.91}$ [7] and pure Fe [8] by using the Eshelby–Kröner model [8]. For the combined 5 1 1/3 3 3 reflection, the constants for the 5 1 1 and the 3 3 3 reflections, as obtained from Equations 3 and 4, were averaged using the multiplicity factors of the lattice planes as weighing factors

		TiC		Fe–C
		422	511/333	211
S_1^{hkl}	(10^{-6} MPa^{-1})	−0.434	−0.414	−1.25
$\frac{1}{2}S_2^{hkl}$	(10^{-6} MPa^{-1})	2.68	2.62	5.71
E	(GPa)	449		212
ν		0.191		0.291
α	(10^{-6}) (K^{-1})	7.6 [9]		see Section 4

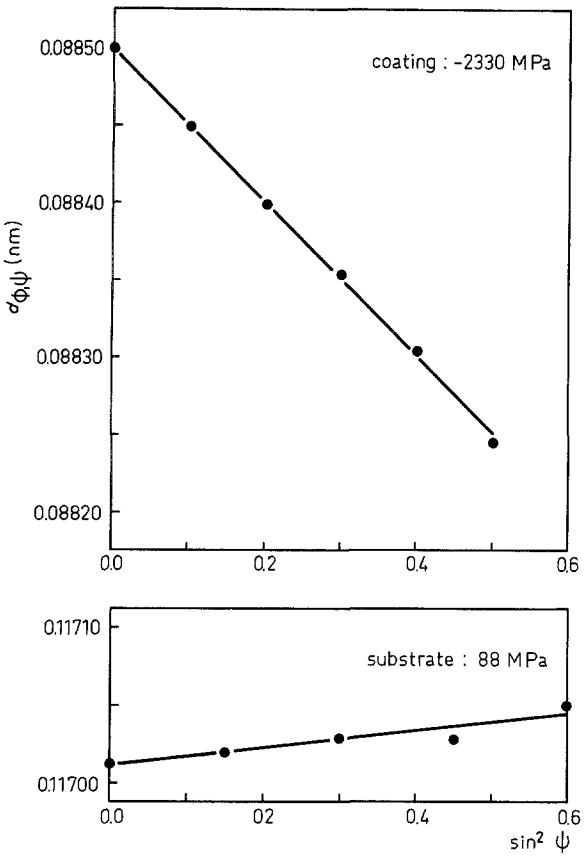

Figure 2 $d_{\phi,\psi}$ against $\sin^2\psi$ for the 422-Cu$K\alpha$ reflection of a TiC coating and for the 211-Cr$K\alpha$ ferrite reflection of its Fe–C (0.27 wt % C) substrate. Deposited with CH_4 in the gas phase.

The measured profiles were corrected for (i) the dead time of the counting system, (ii) a linear background fitted to the extremities of the profile recorded, (iii) the angle-dependencies of Lorentz-polarization [10] and absorption factors, and (iv) the presence of $K\alpha_2$ radiation [11]. Thereafter, the peak positions were determined by fitting a parabola to the peak region of the profiles. Systematic (small) errors in the peak positions, due to defocusing (increasing with increasing ψ), were eliminated by calibration against stress-free reference samples. From the peak positions thus found, the lattice spacings were calculated.

4. Results

4.1. Residual stresses in the TiC coatings

Large compressive stresses are present in all TiC coatings (Table III). The results from the 422-Cu$K\alpha$ and the 511/333-Co$K\beta$ reflections are the same within the experimental error, indicating a consistent data evaluation.

The stress in the TiC coatings parallel to the coating/substrate interface depends on the carbon content of the substrate (cf. Table III). There is practically no difference in stress between TiC coatings deposited with and without CH_4 in the gas phase. The main differences between the TiC coatings deposited with and without CH_4 are the coating thickness and the degree of preferred orientation of the crystallites (texture). The coating thickness increases with the carbon content of the substrate (Table III), and is

TABLE II Conditions for X-ray diffraction measurements

	TiC coating		Ferrite substrate
Reflection	422-Cu$K\alpha$	511/333-Co$K\beta$	211-Cr$K\alpha$
X-ray tube operated at	50 kV, 25 mA	45 kV, 22 mA	55 kV, 20 mA
Divergence slit	1°	0.781°	1°
Receiving slit	0.05 °2θ	0.137° 2θ	0.15° 2θ
2θ range	117–127°	145–159.9°	150–162°
2θ step size at $\omega = 0$	0.04°	0.10°	0.05°
at $\omega > 0$	0.05°	0.10°	0.05°
Counts at peak	~3000	~1500	~2000
Diffractometer (Siemens)	D500	F	D500

larger for coatings deposited in the presence of CH_4 than for coatings deposited in the absence of CH_4. Texture analyses have shown that in all TiC coatings a weak to moderate ⟨1 1 0⟩-fibre texture is present and that in TiC coatings deposited in the presence of CH_4 also a weak, secondary ⟨3 2 1⟩-fibre texture component exists (see also [12]). It appears that, for the same substrate, both coating thickness and texture have no effect on the residual stress in the TiC coatings investigated.

A stress gradient in the present TiC coatings is unlikely because: (i) the $d_{\phi,\psi}$ against $\sin^2\psi$ plots yield a straight line in all cases (cf. Fig. 2) (penetration depth decreases with increasing ψ) and (ii) it was experimentally verified that for different coating thicknesses on the same substrate the same stress is found (cf. Table III with CH_4 versus without CH_4). This was consistent with the finding that the carbon concentration is almost constant over the thickness of the TiC coatings [13].

4.2. Residual stresses in the Fe–C substrates

Because of the absorption of the X-rays by the TiC coating, substrate-stress measurements could not be performed if the coating thickness exceeded about 12 μm. So only substrates with a low carbon content were analysed (cf. Table III). The substrates show a very small tensile stress in the region adjacent to the TiC coating (Table IV). It was expected that the stresses in the substrates with a higher carbon content were of the same order of magnitude. This was confirmed by an additional experiment performed with a substrate of high carbon content (1.0 wt % C, see Table IV), where the coating thickness was about the limiting value of 12 μm (see above).

5. Discussion

5.1. Development of thermal stresses and strains

Stresses in coating and substrate develop during cooling from the deposition temperature (1273 K) to room temperature by the difference in thermal shrink between the TiC coating and the Fe–C substrate. At the deposition temperature the Fe–C alloys are austenitic. On cooling, a "normal" thermal shrink of the Fe–C alloy occurs until, at a certain temperature (depending on the carbon content of the alloy), in the hypo-eutectoid alloys ferrite and in the hypereutectoid alloys cementite starts to form. On further cooling these processes continue until, at the eutectoid temperature, all remaining austenite transforms to pearlite [14]. The total result of these phase transformations, which occur in a temperature range, is a volume increase of the alloy. During further cooling to room temperature a "normal" thermal shrink occurs again. For all Fe–C alloys investigated, cooling from the CVD temperature to room temperature yields a net shrink (see also Fig. 3). TiC experiences only a "normal" thermal shrink.

In the absence of delamination, the difference in thermal shrink between coating and substrate has to be bridged at the coating/substrate interface. The TiC coatings are very thin as compared with the substrates. Then, according to a simple model based on elastic accommodation of strains, mechanical equilibrium and a homogeneous stress distribution in

TABLE III Experimental stresses ($\sigma_\parallel$, see Equation 2), experimental strains ($\varepsilon_\parallel$, see Equation 7) and calculated strains (thermal strain $\varepsilon_\parallel^{th}$, see Section 5.1), parallel to the coating/substrate interface, in CVD TiC coatings of thickness t on Fe–C substrates. Relative errors are indicated

Carbon content substrate (wt % C)	$\varepsilon_\parallel^{th}(10^{-3})$	TiC deposited *without* CH_4				TiC deposited *with* CH_4				Reflection (hkl)
		$\sigma_\parallel$ (MPa)	$\varepsilon_\parallel$ (10^{-3})	$\frac{\varepsilon_\parallel - \varepsilon_\parallel^{th}}{\varepsilon_\parallel^{th}}$ (%)	t (μm)	$\sigma_\parallel$ (MPa)	$\varepsilon_\parallel$ (10^{-3})	$\frac{\varepsilon_\parallel - \varepsilon_\parallel^{th}}{\varepsilon_\parallel^{th}}$ (%)	t (μm)	
0.06 ± 0.01	−5.11	−2270	−4.09	20	1.6	−2330	−4.20	18	2.4	422
0.27 ± 0.01	−5.28	−2300	−4.14	21	7.1	−2330	−4.19	21	9.2	422
		−2420	−4.37	17		−2350	−4.23	20		511/333
0.48 ± 0.02	−6.04	−2715	−4.89	19	13.5	−2530	−4.56	24	14.9	422
0.76 ± 0.04	−6.46	−3100	−5.59	14	15.9	−3030	−5.46	16	20.0	422
0.93 ± 0.05	−6.90	−3240	−5.85	15	17.3	−3120	−5.63	18	23.5	422
		−3170	−5.72	17		−3110	−5.60	19		511/333
1.2 ± 0.06	−8.70	−3280	−5.90	32	21.6	−3180	−5.73	34	27.8	422
Error:	±5%	±2%	±2%	–	±5%	±2%	±2%	–	±5%	–

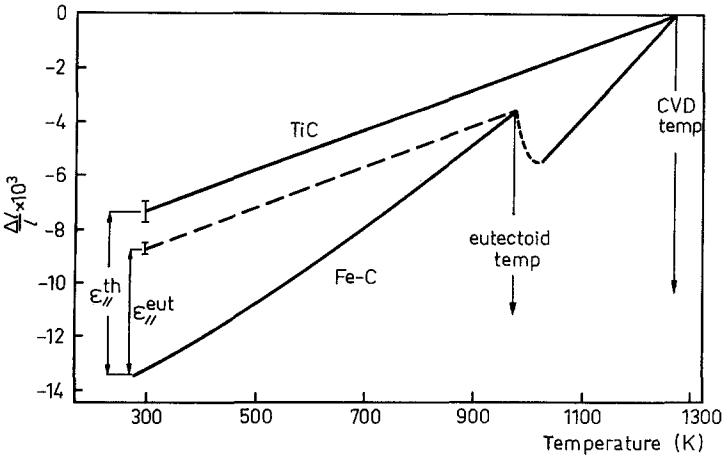

Figure 3 Relative shrink, $\Delta l/l$, of TiC (see Table I) and of an Fe–C alloy with 0.48 wt % C [16] during cooling from the deposition temperature to room temperature. The expected strain, $\varepsilon_{\parallel}^{th}$, and the strain, $\varepsilon_{\parallel}^{eut}$, that would occur if the coating/substrate assembly was strain-free at the eutectoid temperature, are indicated.

both coating and substrate [15], it follows that the difference in thermal shrink between coating and substrate will be predominantly assimilated by the coating.

The net shrink of the Fe–C alloys is larger than of TiC (cf. Fig. 3) and therefore, a compressive stress is expected in the coatings. This agrees with the experiments (see Table III). For a quantitative comparison with the experiments the expected strain in the coating, $\varepsilon_{\parallel}^{th}$, is calculated as depicted in Fig. 3 (the coating/substrate composite is assumed to be strain-free at the deposition temperature). The carbon-content dependent shrink of the substrates was taken into account using literature data [16]. The results are gathered in Table III. The theoretically predicted thermal strain, $\varepsilon_{\parallel}^{th}$, increases with the carbon content of the substrate. This is mainly due to the decrease of the volume change during the phase transformations with increasing carbon content.

In Table III the expected strains, $\varepsilon_{\parallel}^{th}$, are compared with the experimental strains, $\varepsilon_{\parallel}$. For that comparison not the macrostrain at $\psi = 90°$ of the (hkl) lattice spacing ($\varepsilon_{\psi=90°}^{hkl}$ in Equation 1), but the macroscopic strain, $\varepsilon_{\parallel}$, i.e. an average over all crystallites, is needed. This is simply related to the experimental stress, $\sigma_{\parallel}$, by

$$\varepsilon_{\parallel} = \frac{1 - \nu}{E} \sigma_{\parallel} \qquad (7)$$

where ν is the Poisson ratio and E is the Young's modulus of the coating (see Table I).

The experimental residual strain, $\varepsilon_{\parallel}$, in the TiC coating is 14 to 34% smaller than the theoretical estimate, $\varepsilon_{\parallel}^{th}$ (cf. Table III). The substrate region adjacent to the TiC coating assimilates only 2 to 5% of the theoretical thermal strain, $\varepsilon_{\parallel}^{th}$ (cf. Table IV). Hence, in all cases the experimental residual strain in the TiC coatings is smaller than the expected, theoretical strain.

5.2. Relaxation

After cooling, neither fracture nor delamination of the TiC coatings was observed (according to light microscopical as well as scanning-electron microscopical analysis). Then, it can be concluded from the difference between the theoretical and experimental strains that stress relaxation has occurred.

Relaxation induced by (recovery) processes in the TiC coating is not likely since the yield strength [17] and hardness [18] of TiC are high at the temperatures occurring during the experiments. On the other hand the substrates have a low yield strength at the higher temperatures of the experiments [19].

It is assumed that stress relaxation is predominantly caused by the phase transformations occurring in the substrates on cooling, cf. [3]. This is sustained by Fig. 4, where the experimental strain $\varepsilon_{\parallel}$, (Equation 7) and the strain $\varepsilon_{\parallel}^{eut}$, that occurs if the coating/substrate composite would be strain-free at the eutectoid temperature (i.e. after the completion of the phase transformations (see Fig. 3)) are plotted against the carbon content of the substrate [16]. $\varepsilon_{\parallel}^{eut}$ is nearly independent of the carbon content of the substrate. Clearly, a fair agreement between $\varepsilon_{\parallel}$ and $\varepsilon_{\parallel}^{eut}$ exists (Fig. 4). For the TiC coatings on the low carbon content substrates $\varepsilon_{\parallel}^{eut}$ is a little larger than the experimental strain (Fig. 4), so some stress relaxation after the phase transformations is not to be excluded in those cases.

For the TiC coatings on substrates containing 0.76, 0.93 and 1.20 wt % C $\varepsilon_{\parallel}^{eut}$ is somewhat smaller than the experimental strain. In these substrates the formation of grain-boundary cementite, which happens before austenite transforms to pearlite, probably hinders a full relaxation of the instantaneous strains.

TABLE IV Experimental stresses ($\sigma_{\parallel}$, see Equation 2) and experimental strains ($\varepsilon_{\parallel}$, see Equation 7), parallel to the coating/substrate interface, in Fe–C substrates coated with CVD TiC. Errors are indicated.

Carbon content substrate (wt % C)	Fe-C coated *without* CH_4		Fe–C coated *with* CH_4		Reflection (hkl)
	$\sigma_{\parallel}$ (MPa)	$\varepsilon_{\parallel}$ (10^{-3})	$\sigma_{\parallel}$ (MPa)	$\varepsilon_{\parallel}$ (10^{-3})	
0.06 ± 0.01	33	0.11	45	0.15	211
0.27 ± 0.01	68	0.23	88	0.30	211
1.00 ± 0.05	74	0.25	–	–	211
Error:	±10	±0.03	±10	±0.03	–

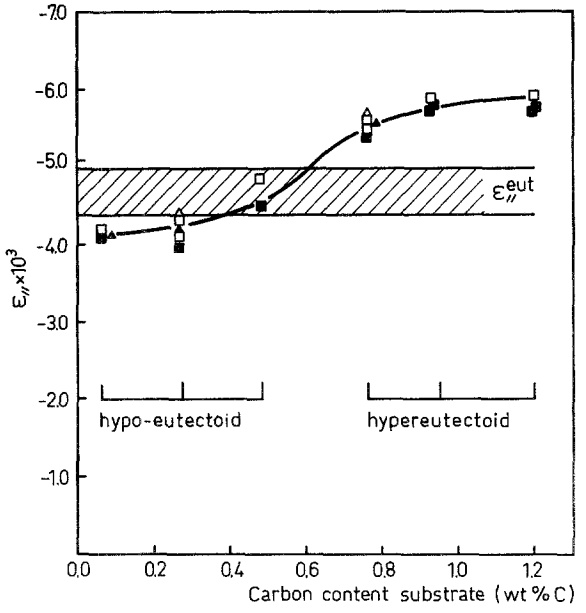

Figure 4 Experimental strains, $\varepsilon_{\parallel}$, in CVD TiC coatings on Fe–C substrates against the carbon content of the substrate. The strain $\varepsilon_{\parallel}^{eut}$ is calculated from the difference in thermal shrink between coating and substrate, that develops during cooling from the eutectoid temperature to room temperature (see section 5.2, last paragraph). (CVD with CH_4: (■) 4 2 2-Cu$K\alpha$ and (▲) 5 1 1/3 3 3-Co$K\beta$; CVD without CH_4: (□) 4 2 2-Cu$K\alpha$ and (△) 5 1 1/3 3 3-Co$K\beta$).

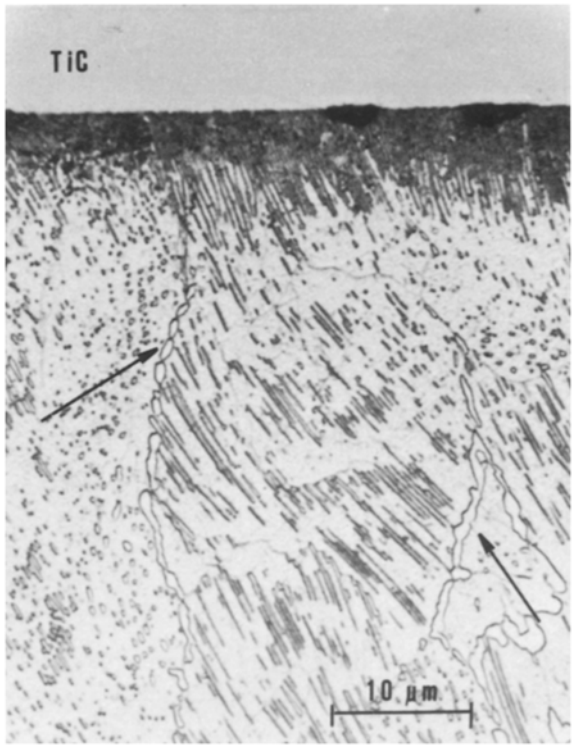

Figure 5 Optical micrograph of a cross-section after nital etching of an Fe–C substrate containing 0.76 wt % C where chromium had diffused into the substrate region adjacent to the TiC coating (chromium originates from the CVD reactor environment). In this region at the grain boundaries an (Fe, Cr)-carbide (arrows) is formed owing to the presence of chromium.

Note that the formation of grain boundary cementite in the substrate containing 0.76 wt % C (see Fig. 5) is caused by the presence of chromium, which shifts the eutectoid composition of the Fe–C system to a smaller carbon content [20]. The chromium, which had diffused into the substrate region adjacent to the TiC coating, originates from the environment in the CVD reactor (see discussion in [13]). The thermal shrink of the substrates is not influenced by the presence of chromium, because the surface region in which it is present (about 5 μm thick) is very small as compared to the thickness of the substrates (see Section 2).

6. Conclusions

Large compressive residual stresses occur in TiC layers chemically vapour deposited on Fe–C substrates. Small tensile residual stresses occur in the substrate region adjacent to the TiC layers.

The stresses in the TiC layers deposited with and without CH_4 in the gas phase are practically the same irrespective of differences in texture and coating thickness.

The stresses are induced by cooling after deposition. The experimental strains are up to 35% smaller than the strains predicted from the difference in shrink between TiC and the Fe–C alloys provoked by the cooling from the CVD temperature to room temperature. Relaxation of the thermal stresses is induced by the phase transformation processes in the substrate region adjacent to the TiC coating. Minor surface modification of substrates (e.g. decarburization or in-diffusion of impurities) may influence the relaxation behaviour significantly.

In coatings on hypo-eutectoid Fe–C substrates all stresses built up by cooling from the CVD temperature to the eutectoid temperature completely relax. This can be ascribed to the phase transformations occurring in the substrate. In coatings on hypereutectoid Fe–C substrates a complete relaxation above the eutectoid temperature is hindered by the formation of grain-boundary cementite.

7. Acknowledgement

The authors wish to thank M. M. Michorius and G. Verspui of Philips Centre for Manufacturing Technology, Eindhoven, for coating the substrates.

Financial support of the Stichting voor Fundamenteel Onderzoek der Materie (FOM) is gratefully acknowledged.

References

1. E. BROSEIT and H. M. GABRIEL, *Z. Werkstofftech.* **11** (1980) 31.
2. H. KRAUSE and H. H. JÜHE, *Härterei Techn. Mitt.* **32** (1977) 302.
3. E. PAULAT, P. LENK and G. WIEGHARDT, *Neue Hütte* **29** (1984) 217.
4. L. CHOLLET, H. BOVING and H. E. HINTERMANN, *J. Mater. Energy Syst.* **6** (1985) 293.
5. G. GILLE and K. WETZIG, *Thin Solid Films* **110** (1983) 37.
6. V. M. HAUK and E. MACHERAUCH, *Adv. X-ray Anal.* **27** (1983) 81.
7. R. CHANG and L. J. GRAHAM, *J. Appl. Phys.* **37** (1966) 3778.
8. F. BOLLENRATH, V. HAUK and E. H. MÜLLER, *Z. Metallkde.* **58** (1967) 76.
9. Y. S. TOULOUKIAN, R. K. KIRBY, R. E. TAYLOR and T. Y. R. LEE, in "Thermal Expansion: Non-metallic Solids," "Thermophysical Properties of Matter", Vol. 13 edited

by Y. S. Touloukian and C. Y. Ho (IFI/Plenum, New York--Washington, 1977) p. 891.
10. R. DELHEZ, E. J. MITTEMEIJER, Th.H. de KEIJSER and H. C. F. ROZENDAAL, *J. Phys. E.* **10** (1977) 784.
11. R. DELHEZ and E. J. MITTEMEIJER, *J. Appl. Cryst.* **8** (1975) 609.
12. P. P. J. RAMAEKERS, G. F. BASTIN, W. G. SLOOF, Th.H. DE KEIJSER and R. DELHEZ, *Vacuum* **36** (1986) 19.
13. W. G. SLOOF, P. P. J. RAMAEKERS, G. F. BASTIN, R. DELHEZ and Th.H. de KEIJSER, to be published.
14. O. KUBASCHEWSKI, in "Iron-Binary Phase Diagrams" (Springer-Verlag, Berlin, 1982) p. 24.
15. C. F. POWELL, J. H. OXLEY and J. M. BLOCHER Jr, in "Vapor Deposition" (John Wiley & Sons, New York, 1966) p. 198.
16. H. ESSER and H. EUSTERBROCK, *Arch. Eisenhüttenw.* **14** (1941) 341.
17. G. E. HOLLOX, *Mater. Sci. Eng.* **3** (1968/69) 121.
18. D. L. KOHLSTEDT, *J. Mater. Sci.* **8** (1973) 777.
19. H. E. HORNBOGEN, in "Physical Metallurgy" edited by R. W. Cahn and P. Haasen (North-Holland, Amsterdam, 1983) p. 1115.
20. G. A. ROBERTS, J. C. HAMAKER Jr and A. R. JOHNSON, in "Tool Steels" (American Society for Metals, Ohio, 1962) p. 200.

Received 12 June
and accepted 18 August 1986